Bushra A. Hasan
Ahmad A. Hasan

Department of Physics, College of Science, University of Baghdad, Baghdad, IRAQ

Synthesis and Characterization of $(TiO_2)_{1-x}(WO_3)_x$ Composites

We report about multilayer $(TiO_2)_{1-x}(WO_3)_x$ thin films with various tungsten oxide concentration deposited on glass substrate via pulsed laser deposition (PLD) technique method. The structural, optical and dielectric properties of the prepared thin films were characterized using x-ray diffraction method (XRD) and UV-Visible absorption spectrometry and LRC meter. The x-ray results showed a polycrystalline structure of pristine titanium oxide and the peaks are identical with the rutile phase and trace of the anatase phase. These peaks are identical with titanium oxide and triclinic tungsten oxide as WO_3 is added to TiO_2 while it was observed that all peaks belong to tungsten oxide at x=1.0. The optical measurements showed a direct E_g^{opt} energy gap of 3.0 eV of the pristine titanium oxide, which showed a non-regular reduction to 1.2 eV with an increase in the content from x = 0.0 to x = 0.6. The "s'' value and the density of states at the Fermi level were found to be increased by increasing the tungsten oxide content up to x=0.8 and then changed and vice versa.

Keywords: Titanium dioxide; Tungsten trioxide; Pulsed-laser deposition; Optical properties
Received: 27 October 2023; **Revised:** 19 November; **Accepted:** 26 November 2023

1. Introduction

Tungsten oxide WO_3 is regarded as one of the most promising inorganic materials due to its possessing of unique properties [1,2], which lead to introduce it in many applications such as solar cells, optical modulation, flat panel displays, reading–erasing optical devices and gas humidity and temperature sensors, etc. [3-10]. It is well known that titanium oxide declared superior photo-responsive properties [11] and many scientists tried to enhance the performance of coloration of WO_3 thin-film by introducing titanium oxide TiO_2 [12,13]. This work investigates the effect of tungsten oxide on TiO_2/WO_3 composite thin films on the comprehensive properties such as structural, optical and electrical properties. The low conversion efficiency of TiO_2 as a result of possessing a wide band gap in the range (3-3.2eV) and high recombination time of photo-induced charge carriers that limit its applications in solar cells [14]. Therefore, great efforts have been achieved to enhance its performance, among them was coupling with another metal oxide such as WO_3 that lead to high photoactivity than pristine TiO_2 [15,16]. This happens due to the small band gap of WO_3 (2.5-2.8 eV) extending strong absorption in the region within the solar spectrum [17].

Paipitak et al. [18] fabricated titanium-doped tungsten oxide with various content using the spin coating method on florin-doped tin oxide (FTO) substrates and subjected them into annealing at a temperature of 500°C. The impact of doping ratio on the structural and optical properties was investigated and showing that the structure of WO_3 was modified and improved the electrochromic performance.

Vasilaki et al. [19] synthesized anatase titanium oxide and monoclinic tungsten oxide WO_3 as a photoconductive cell using sol-gel method. They proved that the bilayers exhibited superior photoactivity compared to that of pristine TiO_2 films with WO_3 acting as an electron trap, resulting in more efficient electron–hole separation and inhibiting their recombination.

Cheng et al. [20] fabricated WO_3/TiO_2 composite nanotubes by the combination of the sol-gel chemical method and the anodic aluminum oxide (AAO) templating method. The diameter of the WO_3/TiO_2 composite nanotubes is about 100 nm, which is in good agreement with the pore diameter of the AAO template. They found that composite nanotubes consisted of mixed oxides of W^{6+} and Ti^{4+}. This research aimed to shed light upon the effect of WO_3 content on the structural, optical and dielectric properties of $(TiO_2)_{1-x}(WO_3)_x$ composites.

This work aimed to made comprehensive study about the influence of WO_3 content on the hole properties of $(TiO_2)_{1-x}(WO_3)_x$ composites .Thus, $(TiO_2)_{1-x}(WO_3)_x$ composites and then thin films were synthesized and the crystal structure were examined. This study also evaluate the energy gap, optical constants, a.c. conductivity, dielectric constant and dielectric loss, and density of states. The optical energy gap is shown to be controlled through the tungsten oxide concentration.

2. Experimental Part

In order to synthesize $(TiO_2)_{1-x}(WO_3)_x$ composites with high purity titanium dioxide (TiO_2) and tungsten trioxide (WO_3) in certain ratios (x=0.0, 0.2, 0.4, 0.6, 0.8 and 1.0) were put in an ampule with dimensions; of length ~25cm and internal diameter ~8mm evacuated to about (~10^{-5} Torr). The mixtures are sintered at 1000°C for 5 hours. The product was grinded and pressed in the shape of a disc thickness of 0.1 cm and diameter of 1 cm. The pulsed-laser deposition technique was adopted to fabricate thin films. The deposition process was performed using

a Q-switched Nd:YAG laser with second harmonic generation (SHG) at wavelength of 532nm in vacuum of $2x10^{-2}$ Torr (energy, pulsed and frequency of 400 mJ, 200 and 6 Hz, respectively). The laser beam was focused through a window on the target. The ablated atoms incident on the glass substrates created the thin films. The measured absorbance and transmittance using the UV-visible-NIR spectrophotometer in a wavelength range of 100-1200 nm. The XRD measurements were conducted at the Ministry of Science and Technology Laboratories using Shimadzu 6000 X-ray diffractometer with Cu-Kα (λ= 1.5404Å) radiation, operated at 30 kV, and 20 mA. Dielectric properties were measured using Hewlett Packard HP4274A & HP4275A devices to obtain the direct resistance, capacitance and dissipation factor "tanδ'' as a function of frequency in the range 50 Hz to 50 MHz by applying a constant voltage (1V).

3. Results and Discussion

The XRD patterns of $(TiO_2)_{1-x}(WO_3)_x$ thin films deposited with various composition ratios are shown in Fig. (1). From this figure, the whole diffraction peaks present in the composite thin films at x=0.0 to x=0.8 identified with rutile TiO_2 at 2θ = 27.39°, 27.43°, 27.35°, 27.23°, which confirm a formation of TiO_2 rutile phase. These peaks disappeared at x=1.0. Only a small peak was identified to anatase TiO_2 located at 2θ = 25.33°. This peak began to vanish with further addition of WO_3 till it disappeared at x=0.6.

Titanium belongs to the IVA group of elements and, as many other metals, is able to form a wide range of oxides. Titanium(IV) dioxide (titania) exists in three common crystalline phases: rutile, which is the thermodynamically stable phase, and the metastable phases anatase and brookite. For anatase phase the band gap energy is 3.2 eV; while the band gap energy of rutile phase is 3.0 eV [21]. Thus the disappearing of anatase phase attributed to that is not stable and is transform to rutile phase also the energy gap value as seen later confirm the rutile phase of the prepared thin films.

Figure (1) also shows many peaks that belong to the triclinic phase of WO_3 when this oxide was added to TiO_2. One can observe the diffraction peaks of WO_3 at 23.05°, 23.70°, 28.73°, 33.56° and 34.13° which indexed to the planes (001), (020), (200), $(\bar{1}11)$, $(02\bar{1})$ and $(2\bar{2}0)$ of the monoclinic WO_3 phase, respectively. The peak positions are compatible with the standard card number (JCPDS card no. 72-1465) [22].

On the other hand, the height of peaks of TiO_2 is decreased which means that the degree of crystallinity decreased for x=0.2 to 0.6. This observation explains the reduction of crystal size of the main plane of crystal growth. The crystal size decreased from 40.3 to 20.2 nm by increasing the tungsten oxide from x=0.0 to 0.6. Increasing the ratio of tungsten oxide into titanium oxide leads to grow up the peaks height of the tungsten oxide and dominated a part of the peaks height of the titanium oxide by changes the plane of crystal growth from (110) to (001) and (020). The crystal size of the preferred planes (001) and (020) value changed from (20, 11.8nm), (22.2, 6.7nm), (22.2, 28.6nm), (25, 25nm) and (28.6, 25.6nm) for x=0, 0.2, 0.4, 0.6, 0.8 and 1.0 respectively.

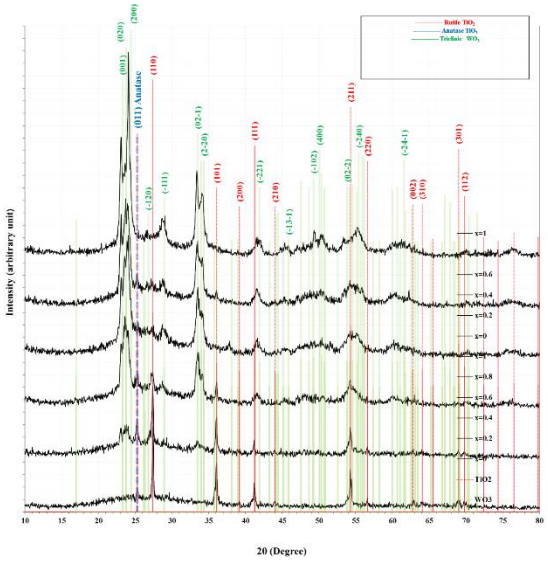

Fig. (1) XRD patterns of $(TiO_2)_{1-x}(WO_3)_x$ thin films composites as rutile (red pattern), anatase (blue) and triclinic of WO_3 (green)

Figure (2) shows the transmittance as a function of the wavelength of $(TiO_2)_{1-x}(WO_3)_x$ composite thin films. It can be observed that the transmittance grows up with the addition of tungsten oxide to starting material which indicates a reduction of the reflection and absorption as well as, indicates that introducing the tungsten oxide makes the fabricated sample more transparent and less absorbance.

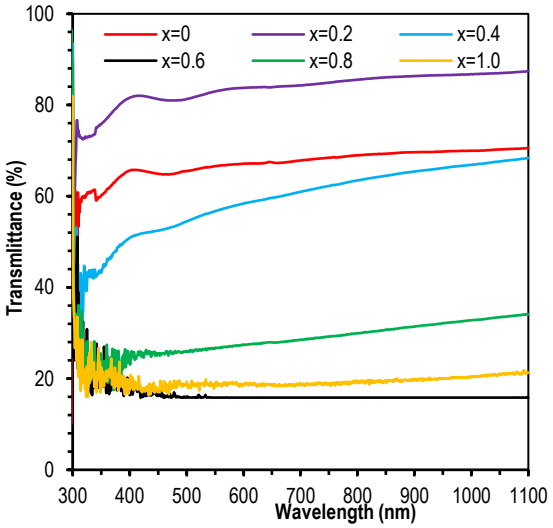

Fig. (2) Transmittance spectra of deposited $(TiO_2)_{1-x}(WO_3)_x$ composite thin films for a range of x content

The transmittance then gets reduced with increased tungsten oxide content till it reaches a minimum value at x=0.6.The minimum transmittance

corresponded to maximum absorbance as shown from table (2) is related with the domination of the tungsten oxide upon the titanium oxide. The maximum absorbance is related with the new stated created by the tungsten oxide in the band gap. After that, the transmittance increased again with a further increase of tungsten oxide content. The reduction of transmittance referred to grow in the reflection and absorption values indicates that the addition of tungsten oxide increases the opacity of the fabricated samples. The shifts of transmittance toward longer wavelengths (lower energies) accompanied by the increment of tungsten oxide content are also related to structural change.

The Tauc equation adopted to estimate the energy gap of the fabricated samples. The plot of $(\alpha hv)^{1/r}$ as a function of energy (hv) is shown in Fig. (3). The value of the optical energy gap of titanium oxide is 3.0 eV, which extracted from linear fit in figure 3. The optical energy gap shows a regular reduction or red shift as tungsten oxide added to titanium oxide. Moreover, the optical energy gap decreased from 3.0 to 1.2 when tungsten oxide content increased from x=0.0 to 0.6.

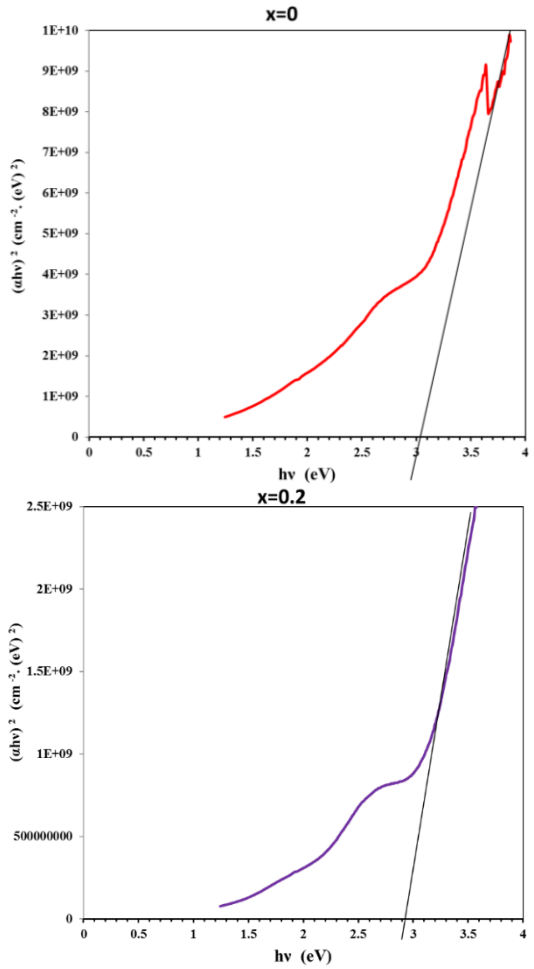

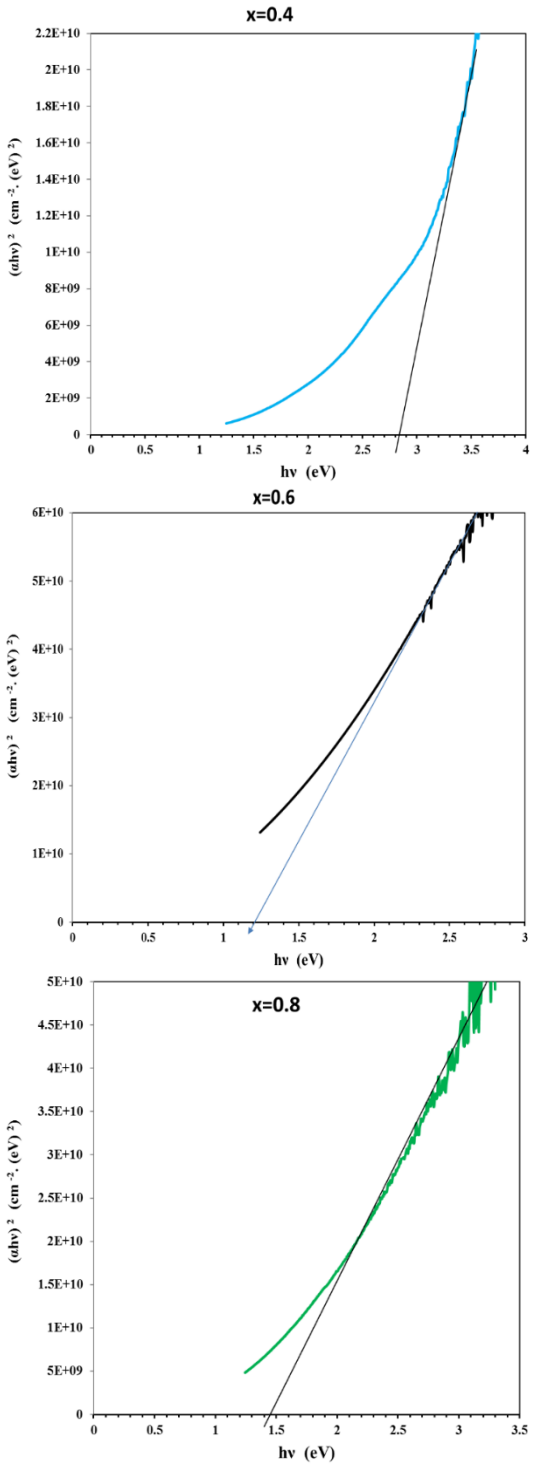

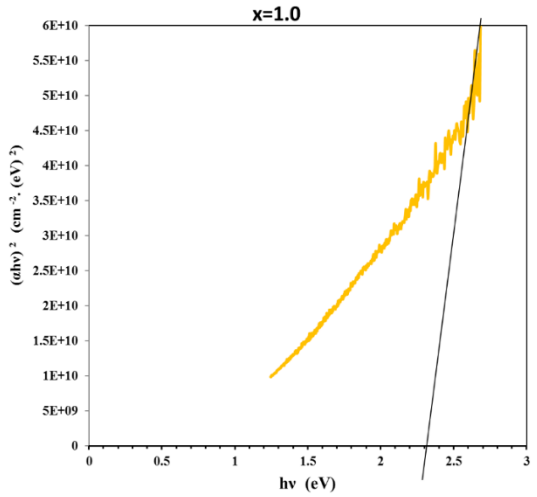

Fig. (3) Variation of $(\alpha h\nu)^2$ with $h\nu$ for $(TiO_2)_{1-x}(WO_3)_x$ thin films for a range of x content

Indeed E_g^{opt} increased from 1.2 to 2.3 eV which blue shifting of energy gap by increasing the tungsten oxide content from x=0.6 to 1.0. This expected since the energy gap of titanium oxide is wider than tungsten oxide [23,24]. The energy gap reduction of pristine WO_3 compared to the published value can be attributed to that hydrogen adsorption or loss of oxygen from the surface. Bringans et al. [25] carried out the UV photoemission measurements of the (001) surface of WO_3. They showed that after exposure to atomic hydrogen new states appear in the energy gap region at 2.3 and 0.9 eV below the Fermi energy.

Figure (4) shows the spectrum of the refractive index as a function of wavelength for $(TiO_2)_{1-x}(WO_3)_x$ films for a range of x content (0.0, 0.2,0.4,0.6,0.8, and 1.0). It observed from this figure and table (2) that the refractive index decreases irregularly with the addition of tungsten oxide. Figure (5) shows the variation trend of the extinction coefficient of the $(TiO_2)_{1-x}(WO_3)_x$ films, while figures (6) and (7) show the wavelength-dependent spectra of (ε_r) and (ε_i) for $(TiO_2)_{1-x}(WO_3)_x$ films.

The findings suggest that the energy band gap of $(TiO_2)_{1-x}(WO_3)_x$ composites thin films as well as the optical constants can be controlled by adjusting WO_3 concentration; the absorption coefficient rh the most high value which related with maximum extinction coefficient value at x=.6 and shift of energy gap to low energy side (1.2eV).

Table (2) Values of E_g^{opt} and optical constants at λ=550 nm for $(TiO_2)_{1-x}(WO_3)_x$ composites thin films

x	T%	α (cm⁻¹)	k	n	ε_r	ε_i	Eg (eV)
0.0	66.60	20324	0.089	2.316	5.355	0.412	3.0
0.2	82.99	9327	0.041	1.851	3.426	0.151	2.9
0.4	56.73	28350	0.124	2.520	6.337	0.626	2.8
0.6	15.85	92120	0.403	1.512	2.123	1.220	1.2
0.8	26.66	66119	0.290	2.328	5.336	1.348	1.45
1.0	19.03	82977	0.363	1.851	3.295	1.345	2.3

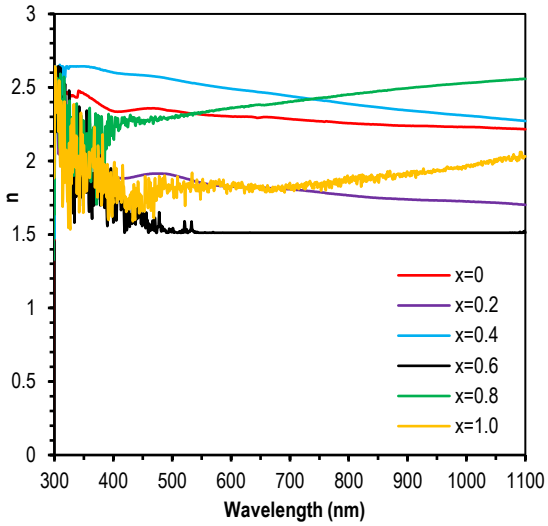

Fig. (4) Variation of refractive index with the wavelength of deposited $(TiO_2)_{1-x}(WO_3)_x$ composites thin films

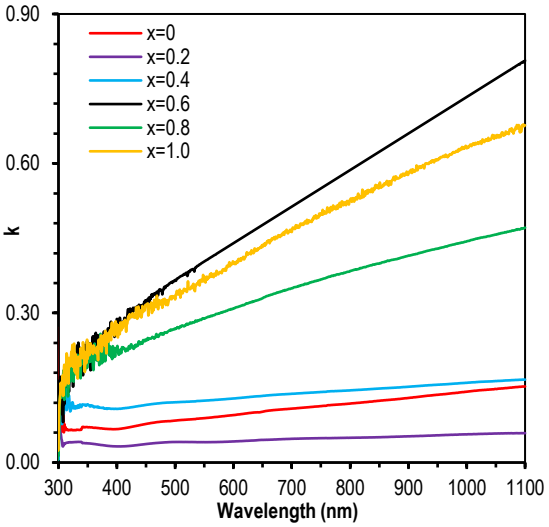

Fig. (5) Variation of extinction coefficient with the wavelength of $(TiO_2)_{1-x}(WO_3)_x$ composites thin films

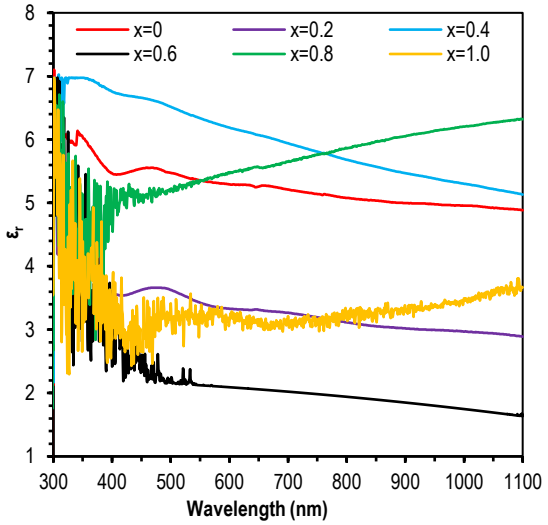

Fig. (6) Variation of real dielectric constant with the wavelength of $(TiO_2)_{1-x}(WO_3)_x$ composite thin films for a range of x content

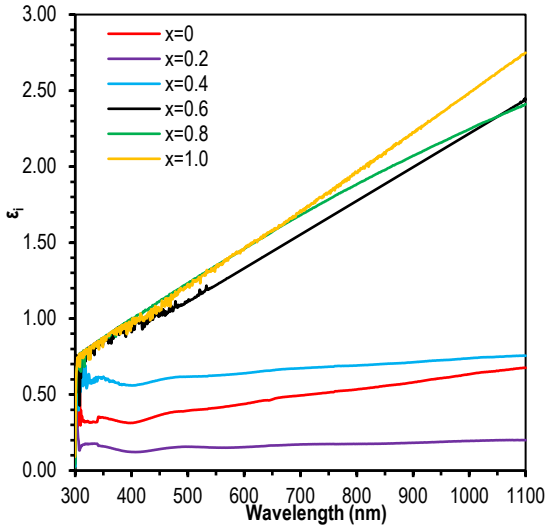

Fig. (7) Variation of the imaginary dielectric constant with the wavelength of $(TiO_2)_{1-x}(WO_3)_x$ composites thin films

Fundamentally total conductivity $\sigma_{tot}(\omega)$ is the summation of direct current conductivity $\sigma_{d.c}(\omega)$ and alternative current $\sigma_{ac}(\omega)$. So the last term can be written as $\sigma_{a.c}(\omega)=A\omega^S$, where S, A, and ω represent the frequency exponent, a constant, and the angular frequency ($\omega=2\pi f$). The frequency dependence of $\sigma_{ac}(\omega)$ of $(TiO_2)_{1-x}(WO_3)_x$ composites that measured in the frequency range 50Hz-50MHz as shown in Fig. (8). It is observed that $\sigma_{a.c}(\omega)$ grows up by increasing angular frequency except for pristine TiO_2. As well as, $\sigma_{a.c}(\omega)$ increases by increasing the tungsten oxide up to x=0.8 and then reduced. The "S'' values were calculated from the equation $\mathrm{Ln}[\sigma_{a.c}(\omega)]/\mathrm{Ln}(\omega)$, where the values of "$S$'' are listed in table (3). The small values of "S'' refers to the hopping mechanism [26], but the values of "S'' grows by the addition of tungsten oxide up x=0.8 and then reduced. The growth of "S'' values postulated that small polaron (SP) is the most convenient model that can explain the behaviour of "S'', while the correlated barrier hopping (CBH) model is a convenient model for the reduction in the value of "S''. The density of localized states at the Fermi level calculated by using the following relation [27]:

$$\sigma_{a.c}(\omega)=\frac{1}{3}\pi e^2 k_B T[N(Ef)]^2\bar{\alpha}^{-5}\omega[\ln(\nu ph)\omega]^4 \quad (1)$$

where e, ν_{ph}, and $\bar{\alpha}$ are the electronic charge, the predominant phonon frequency and the exponential decay parameter of the localized states wave functions. By assuming ν_{ph} = 10^{12} Hz and $\bar{\alpha}^{-1}$ = 10Å [26-28], $N(E_f)$ is listed in table (3). It is obvious that there is a systematic increase in the density of states by increasing the tungsten oxide up to x=0.8 and vice versa. This result is consistent with the resulting narrowing of the band gap of TiO_2.

The plot of ε_1 and ε_2 against frequency shown in Fig. (9a,b). The two contributions of the dielectric constant ε_1 and ε_2 give the physical meaning of the dissipation factor tanδ, which represents the energy dissipated per cycle/energy sorted per cycle. The dielectric constant ε_1 of $(TiO_2)_{1-x}(WO_3)_x$ with a range of composites ratios is investigated within the employed frequency range of 50Hz-50MHz. It is clear from Fig. (9a) that ε_1 grow up by increasing the WO_3 content up to x=0.8 WO_3 and then decreases. Indeed ε_1 increases from 156 to 6413 when WO_3 content increases from 0 to 0.8 and then decreases to 4586 with a further increase of WO_3. On the other hand, ε_1 tends to decrease by increasing the frequency till reaches minimum values. This is attributed to the certainty that dominates the electrode is blocking layer and hence the dielectric trend is modified by the electrode polarization, while at high frequency the electrode polarization effect has vanished. The increase of ε_1 with WO_3 content attributed to the growth of capacitance (direct relation).

Figure (9b) displays the plot diagram of ε_2 as a function of the frequency of $(TiO_2)_{1-x}(WO_3)_x$ composite with different WO_3 content. It can be observed that the plot is absent from any absorption peak. It is clear from the same figure that ε_2 reduces by increasing angular frequency. The reduction of dielectric loss ε_2 with frequency can be attributed to the fact that the migration of ions is the main origin of the dielectric loss at low frequencies. Thus the dielectric loss ε_2 at low and moderate frequencies is recognized by high values of ε_2 as a result of the participation of ion hopping and conduction loss of ion migration, as well as the contribution of ion polarization loss. However, at high frequencies, the ion vibrations may be the only origin of dielectric loss. The plot diagram of real and imaginary dielectric constant is shown in figure (Cole-Cole diagram) in Fig. (10). The relations produced an arc of the circle where the centre is located below the x-axis. By measuring the angle formed between the diameter of the circle and the x-axis, the (α) was calculated and put in table (3). The value of α exhibits none systematically changing with the tungsten oxide ratio by increasing and decreasing. The increase of α value is due to reducing the intermolecular forces that take place when a potential barrier is formed. While the reduction of α value is due to the increment of intermolecular forces [29-35].

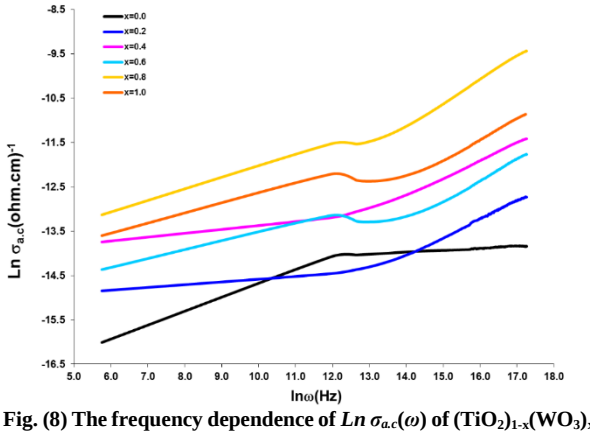

Fig. (8) The frequency dependence of $Ln\ \sigma_{a.c}(\omega)$ of $(TiO_2)_{1-x}(WO_3)_x$ composites with tungsten content

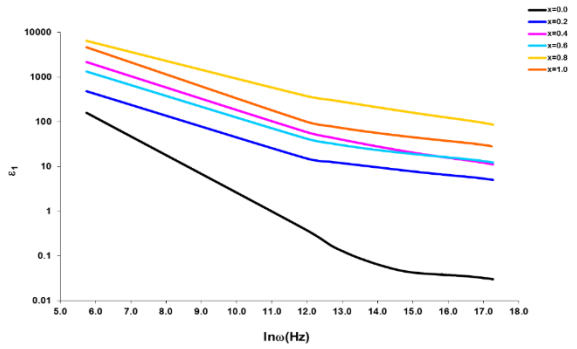

(a)

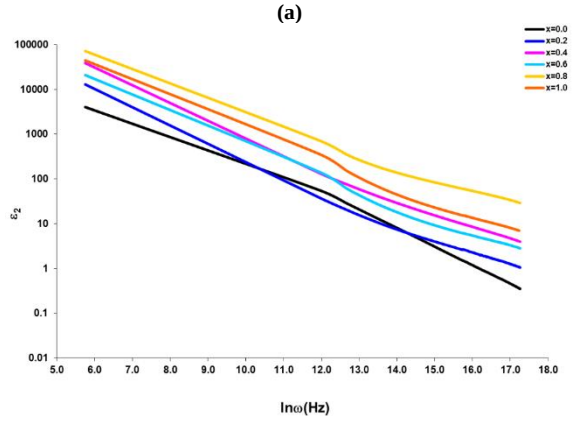

(b)

Fig. (9) (a) The frequency dependence of ε_1 of $(TiO_2)_{1-x}(WO_3)_x$ composites with tungsten content, (b) The frequency dependence of ε_2 versus of $(TiO_2)_{1-x}(WO_3)_x$ composites with tungsten content.

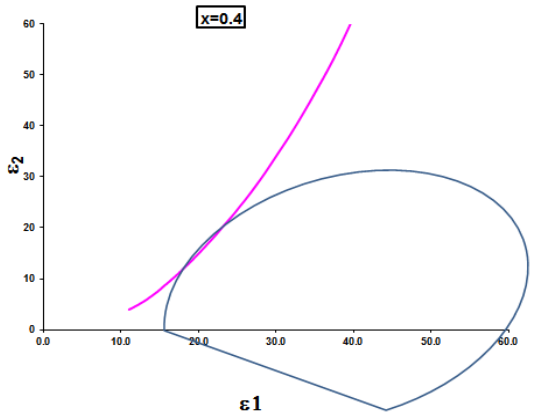

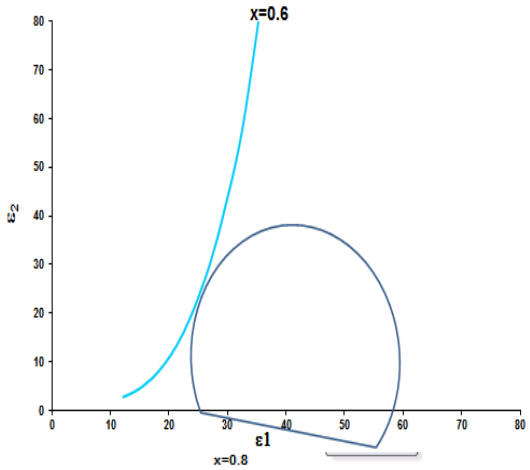

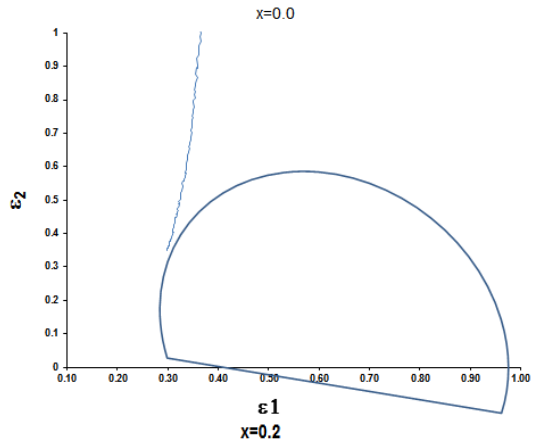

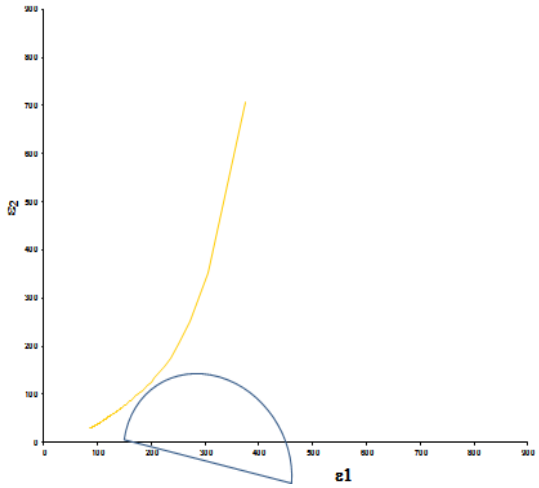

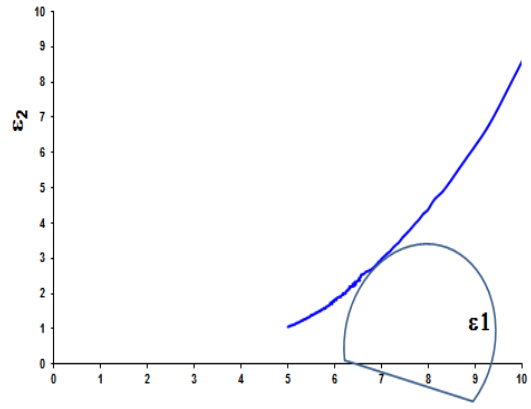

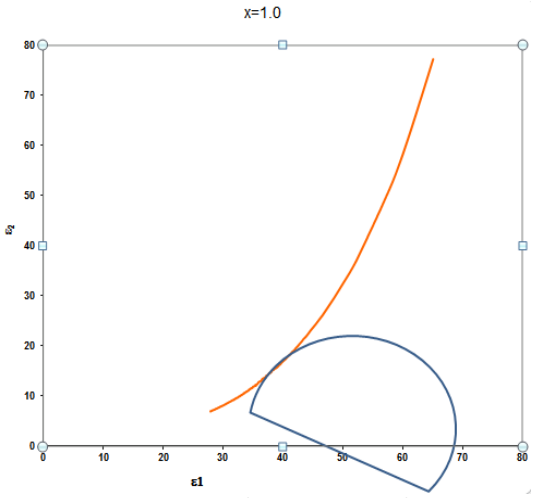

Fig. (10) A plot diagram of ε_1 versus ε_2 of $(TiO_2)_{1-x}(WO_3)_x$ composites with tungsten content

Table (3) Values of "S'', N(Ef) and α based on the x value

x	α	S	$N(E_f)$
0	0.111111	0.1053	6.77165E+34
0.2	0.222222	0.3076	5.26645E+35
0.4	0.255556	0.3105	1.01874E+36
0.6	0.133333	0.3348	1.3306E+36
0.8	0.177778	0.4298	2.74113E+36
1.0	0.277778	0.3348	1.34422E+36

4. Conclusions

$(TiO_2)_{1-x}(WO_3)_x$ composite consists of rutile and trace of secondary anatase phases and monoclinic WO_3, are synthesized by solid-state reaction and pulsed-laser methods. The prepared $(TiO_2)_{1-x}(WO_3)_x$ thin films deposited at ambient temperature have polycrystalline structure for all tungsten oxide content. The crystal size of $(TiO_2)_{1-x}(WO_3)_x$ sample is decreased with the increase of tungsten oxide content up to x=0.6 and vice versa. The increase of tungsten oxide content leads to red shifts up to x=0.6 and then blue shifts take place for further increase of tungsten oxide content. $(TiO_2)_{1-x}(WO_3)_x$ composites films show a high tunable energy gap in the solar spectrum compared to pristine TiO_2 films. This can be attributed to WO_3 acting as an electron trap, which simplifies charge transport and limits charge recombination. It obtained an energy gap in the solar spectrum range that makes the $(TiO_2)_{1-x}(WO_3)_x$ composites eligible for use in solar cell applications. The results show that the polarizability (α) grows when the addition of WO_3 results in forming a barrier or reducing the intermolecular forces while α decreases when the addition WO_3 increases the force of the intermolecular. It is more suitable to use $(TiO_2)_{1-x}(WO_3)_x$ composites as a resistor since α <0.5.

References

[1] L. Zhuang, X.Q. Xu and H. Shen, *Surf. Coat. Technol.*, 167 (2003) 217.
[2] Y.D. Wang et al., *Solid-State Electron.*, 45 (2001) 639.
[3]N. Özer, *Thin Solid Films*, 304 (1997) 310.
[4] A.E. Aliev and H.W. Shin, *Solid State Ion.*, 154/155 (2002) 425.
[5] J. Shieh et al., *Sens. Actuat. B*, 86 (2002) 75.
[6] T. Tatsuma et al., *Langmuir*, 18 (2002) 7777.
[7] S.H. Baeck et al., *Adv. Mater.*, 15 (2003) 1269.
[8] M. Gratzel, *Nature*, 409 (2001) 575.
[9] D.S. Lee et al., *Sens. Actuat. B*, 60 (1999) 57.
[10] X.L. Li, J.F. Liu and Y.D. Li, *Inorg. Chem.*, 42 (2003) 921.
[11] K.Y. Song et al., *Chem. Mater.*, 13 (2001) 2349.
[12] C.A. Linkous et al., *Environ. Sci. Technol.*, 34 (2000) 4754.
[13] T. He et al., *J. Phys. Chem. B*, 106 (2002) 12670.
[14] X. Chen and S.S. Mao, *Chem. Rev.*, 107 (2007) 2891.
[15] H.G. Oliveira et al., *Sci. Adv. Mater.*, 4 (2012) 673.
[16] S. Rawal, S. Bera and W. Lee, *Catal. Lett.*, 142 (2012) 1482.
[17] O. Mashtalir et al., *Int. J. Appl. Ceram. Tech.*, 10 (2013) 26.
[18] K. Paipitak et al., *Energy Procedia*, 9 (2011) 446-451.
[19] E. Vasilaki et al., *Appl. Phys. A*, 123 (2017) 231.
[20] L. Cheng et al., *Nanotechnology*, 16 (2005) 1341-1345.
[21] F. Scarpelli et al., "Mesoporous TiO_2 Thin Films: State of the Art", Ch. 3, IntechOpen (2018) http://dx.doi.org/ 10.5772/intechopen.74244.
[22] **International Tables for X-ray Crystallography,** vol. I, 2nd ed., Birmingham: Kynoch Press (1965).
[23] H. Widiyandari et al., "Optical properties and photocatalytic activities of tungsten oxide (WO3) with platinum co-catalyst addition", *AIP Conf. Proc.*, 1712 (2016) 050027.
[24] W.A. Al-Taa'y and B.A. Hasan, "Structural and Optical Properties of TiO_2:NiO Nanoparticles Thin Films Prepare by Chemical Spray Pyrolysis", *Iraqi J. Phys.*, 19(49) (2021) 22-31.
[25] R.D. Bringans, H. Höchst and H.R. Shanks, *Surf. Sci.*, 111(1) (1981) 80-86.
[26] S. Sathish, B.C. Shekar and R. Sathyamoorthy, *Phys. Proced.*, 49 (2013) 166-176.
[27] L.S. Valor, Ph.D thesis, University of Minnesota (2022).
[28] R. Murti et al., *AIP Adv.*, 6 (2016) 035010.
[29] B.K. Madhavi Yadav et al., *e-Polymers*, 19 (2019) 453-461.
[30] I.M.El Anwar, A.K. Mohamad and F.F. Hammad, *Egypt. J. Chem.*, 425 (1999) 27-44.
[31] B.A Hasan and D.A Umran, "Dielectric permittivity and ac conductivity of CuInSeTe thin films", *Semicond. Sci. Technol.*, 27 (2012) 125014.
[32] B.A. Hasan, D.A. Umran and M.A. Kadhim, "Characterization of CuInSTe/CdS Heterojunctions", *The 6th Sci. Conf. Renew. Ener. Appl., J. Phys.: Conf. Ser.*, 1032 (2018) 012020.

[33] A.A. Hasan, "Dielectric Study of PVC-LiF Composites Films", *Iraqi J. Sci.*, 62(3) (2021) 861-870.
[34] A.A. Hasan, "Synthesis and Dielectric Properties of MgO:ZnO Composites", *Iraqi J. Sci.*, 63(12) (2022) 5232-5241.
[35] B.A. Hasan and H.H. Issa, "Dielectric properties and A.C electrical conductivity analysis of $(La_2O_3)_{1-x}(ZnO)_x$", *2nd Int. Sci. Conf. Al-Ayen Univ. (ISCAU-2020), IOP Conf. Ser.: Mater. Sci. Eng.*, 928 (2020) 072003.

Table (1) XRD data of $(TiO_2)_{1-x}(WO_3)_x$ composite as thin films

Sample	2θ (Deg.)	FWHM (Deg.)	d_{hkl} Exp.(Å)	C.S (nm)	Hkl	Phase
0	25.3302	0.3244	3.5133	25.1	(011)	Anatase TiO_2
	27.3986	0.2027	3.2526	40.3	(110)	Rutile
	36.1182	0.3244	2.4849	25.8	(101)	Rutile
	41.2283	0.2839	2.1879	29.9	(111)	Rutile
	44.0267	0.3650	2.0551	23.5	(210)	Rutile
	54.2874	0.3245	1.6884	27.5	(211)	Rutile
	56.5991	0.2839	1.6248	31.8	(220)	Rutile
	62.8447	0.2839	1.4775	32.8	(002)	Rutile
0.2	23.0591	0.4056	3.8539	20.0	(001)	Triclinic WO_3
	23.7891	0.6894	3.7373	11.8	(020)	Triclinic WO_3
	25.2491	0.3245	3.5244	25.1	(011)	Anatase TiO_2
	27.4392	0.2434	3.2479	33.6	(110)	Rutile
	33.5632	0.8111	2.6679	10.2	(02-1)	Triclinic WO_3
	36.0776	0.2839	2.4876	29.4	(101)	Rutile
	41.2283	0.2839	2.1879	29.9	(111)	Rutile
	44.0672	0.3244	2.0533	26.4	(210)	Rutile
	54.2874	0.3245	1.6884	27.5	(211)	Rutile
	56.5991	0.3245	1.6248	27.8	(220)	Rutile
	62.8447	0.3650	1.4775	25.5	(002)	Rutile
0.4	23.1402	0.3650	3.8406	22.2	(001)	Triclinic WO_3
	23.7080	0.4866	3.7499	16.7	(020)	Triclinic WO_3
	25.3302	0.3245	3.5133	25.1	(011)	Anatase TiO_2
	27.3581	0.4056	3.2573	20.2	(110)	Rutile
	28.7370	0.4867	3.1041	16.8	(-111)	Triclinic WO_3
	33.5226	0.5678	2.6711	14.6	(02-1)	Triclinic WO_3
	34.1309	0.4055	2.6249	20.5	(2-20)	Triclinic WO_3
	36.1182	0.2839	2.4849	29.4	(101)	Rutile
	41.4716	0.6083	2.1756	14.0	(111)	Rutile
	54.2468	0.5678	1.6896	15.7	(211)	Rutile
0.6	23.0591	0.3650	3.8539	22.2	(001)	Triclinic WO_3
	23.5458	0.2839	3.7754	28.6	(020)	Triclinic WO_3
	24.0730	0.4461	3.6939	18.2	(200)	Triclinic WO_3
	28.6964	0.7300	3.1084	11.2	(-111)	Triclinic WO_3
	33.5226	0.4867	2.6711	17.0	(02-1)	Triclinic WO_3
	41.6338	0.5272	2.1675	16.1	(111)	Rutile
	54.3279	1.3383	1.6873	6.7	(211)	Rutile
0.8	23.1402	0.3244	3.8406	25.0	(001)	Triclinic WO_3
	23.7080	0.3244	3.7499	25.0	(020)	Triclinic WO_3
	23.9919	0.3245	3.7062	25.0	(200)	Triclinic WO_3
	25.2086	0.4461	3.5300	18.2	(011)	Anatase TiO_2
	27.2364	0.4867	3.2716	16.8	(110)	Rutile
	28.7370	0.6895	3.1041	11.9	(-111)	Triclinic WO_3
	33.4820	0.4867	2.6742	17.0	(02-1)	Triclinic WO_3
	34.0904	0.4462	2.6279	18.6	(2-20)	Triclinic WO_3
	36.0776	0.4055	2.4876	20.6	(101)	Rutile
	41.6338	0.6894	2.1675	12.3	(111)	Rutile
	54.4902	1.6628	1.6826	5.4	(211)	Rutile
1.0	23.0997	0.2839	3.8473	28.6	(001)	Triclinic WO_3
	24.1136	0.3245	3.6877	25.0	(020)	Triclinic WO_3
	28.7775	0.6489	3.0998	12.6	(-111)	Triclinic WO_3
	33.3604	0.4056	2.6837	20.4	(02-1)	Triclinic WO_3
	34.0904	0.3650	2.6279	22.8	(2-20)	Triclinic WO_3
	41.7149	0.7706	2.1635	11.0	(-221)	Triclinic WO_3
	45.8111	0.6894	1.9791	12.5	(-240)	Triclinic WO_3
	49.3801	0.5273	1.8441	16.6	(-102)	Triclinic WO_3
	50.3129	0.8111	1.8121	10.8	(400)	Triclinic WO_3
	55.2202	0.8923	1.6621	10.0	(-240)	Triclinic WO_3

